Metal β-Diketoiminate Precursor use in Aerosol Assisted Chemical Vapour Deposition of Gallium- and Aluminium-Doped Zinc Oxide

Caroline E. Knapp,[a]* Caragh Dyer,[a] Nicholas P. Chadwick,[a] Rachael Hazael[b] and Claire J. Carmalt[a]

[a] Department of Chemistry, University College London, 20 Gordon Street, Christopher Ingold Laboratories, London, WC1H 0AJ, UK.

[b] Centre for Defence Engineering, Cranfield Defence and Security, Cranfield University, Shrivenham, Swindon, SN6 8LA, UK

Email: caroline.knapp@ucl.ac.uk

Abstract

Aerosol assisted chemical vapour deposition (AACVD) has been used to deposit thin films of ZnO from the single-source precursor [Zn((OC(Me)CHC(Me)N(^{i}Pr))$_2$] (**1**) affording highly transparent (>80%) and conductive films (sheet resistance ~70 KΩ/sq). Extension of this AACVD method whereby related precursors of the type, [R$_2$M(OC(Me)CHC(Me)N(^{i}Pr))] (R = Et, M = Al (**2**); R = Me, M = Ga (**3**)), isolated as oils, were added to the precursor solution allowed for the deposition of aluminium- and gallium-doped ZnO (AZO and GZO) films, respectively. Complexes **1**-**3** were characterised by elemental analysis, NMR and mass spectrometry. Films were deposited in under 30 minutes at 400 °C, from CH$_2$Cl$_2$/toluene solutions with a N$_2$ carrier gas. Herein we report the bulk resistivity, ρ, of AZO (0.252 Ωcm) and GZO (0.756 Ωcm) films deposited from this novel approach. All the films transparency exceeded 80% in the visible, X-ray diffraction (XRD) showed all films to crystallise in the wurzite phase whilst X-ray photoemission spectroscopy (XPS) confirmed the presence of the Al and Ga dopants in the films, and highlighted the low C-contamination (< 5%) this route offers. Investigation of a mechanism analogous to the Kirkendall effect confirmed that heating of GZO films at 1000 °C produced the spinel structure GaZn$_2$O$_4$.

Keywords: Zinc oxide, thin films, Al doping, Ga doping, AACVD

1. Introduction

Metal oxide thin films have garnered a large amount of attention in the scientific community due to their wide range of existing and potential applications, particularly their use in transparent conducting oxide (TCO) coatings.[1] TCOs are optically transparent and electrically conductive making them the ideal candidates for optoelectronic and photovoltaic applications. Currently, the fastest growing use of TCOs is in flat panel display technology, an area that covers computer and smartphone screens for consumer electronics but also for the military and medical industries.[2] There is also great demand for their use in the glass industry particularly in electrochromic windows. TCOs often comprise of *n*-doped tin, zinc or indium oxides. As a

38 general rule, a TCO should possess a transmittance of > 80%, a carrier concentration of 10-20 cm^{-3} and the

39 host matrix must comprise of a wide band gap metal oxide (> 3 eV) and be doped until rendered degenerate

40 to exhibit metallic-like electrical conductivity.[3] However, these desirable properties can conflict as the large

41 band gap required for optical transparency is detrimental to the low resistivity required (~10^{-4} Ωcm), often

42 causing problems for the doping process.

43 Indium tin oxide (ITO) films are the industrial standard with resistivites of ~1×10^{-4} Ωcm, a large bandgap of

44 4 eV and transparency in the majority of the visible region. Indeed, the optical and electrical properties are

45 difficult to match, however alternatives to ITO are widely sought with a view to lowering the cost and

46 simplifying deposition techniques.

47 A range of doped zinc oxides are a viable alternative to ITO.[4] The large bandgap, ease of doping and high

48 conductivity of zinc oxide is consistent with the prerequisites for TCOs however doping is necessary due to

49 the low carrier concentration and thus high resistivity of pure ZnO.[5] The doping of zinc oxide occurs through

50 *n*-type doping where impurities are introduced into the crystal lattice to cause an excess of negative charge

51 carriers. Doped zinc oxides have been widely explored with dopants, such as arsenic,[6] indium[7] and

52 manganese.[8] Arguably, the most notable dopant is aluminium, forming Al-doped ZnO (AZO) which is

53 currently used in the photovoltaic industry, with reported resistivities as low as 2.4×10^{-4} Ωcm and a large

54 band gap of 3.4 – 3.9 eV.[9] Furthermore, although the properties of ITO are considered superior, the low

55 cost, availability and low toxicity of zinc and aluminium are appealing industrially. It was reported that AZO

56 exhibits a high stability at temperatures > 700 K and are the only films stable in a gaseous plasma containing

57 hydrogen[10] also more recently it has been reported that combining both aluminium and gallium as dopants

58 offers a balance between chemical stability and conductivity.[11] Various doping concentrations have been

59 explored in the literature with most lying between 2 – 10 at.%. Muiva *et al.* reported the optimum doping

60 concentration to be 2 at.% for enhanced conductivities and transmittance > 85%.[12]

61 Group III elements are common dopants for ZnO[13] and moving down the group from Al to Ga as a dopant

62 gives Ga-doped zinc oxide (GZO), another alternative to ITO. Studies suggest that gallium doping is more

63 effective than aluminium doping as the lower reactivity of gallium allows it to be easily controlled during the

64 doping process. Additionally, the smaller Ga-O bond length minimises the deformity of the ZnO crystal lattice

65 allowing higher concentrations of the dopant to be introduced into the host matrix. Furthermore, with a

66 reported resistivity between $4-5 \times 10^{-4}$ Ωcm it also offers similarly impressive electrical properties.[14,15] In

67 addition to dopant concentration, electrical properties of films can also depend on film thickness. Fortunato

68 *et al.* discovered that increasing the GZO film thickness also increased the electron mobility as defects are

69 more common in thinner films thus scattering charge carriers. However, saturation of the resistivity occurred

70 at thicknesses that exceeded 500 nm.[15]

71 Recently studies of films of AZO and GZO deposited *via* AACVD showed the correlation between dopant levels

72 and resultant resistivity.[16,17] Commercially procured zinc acetylacetonate, aluminium chloride and gallium

73 chloride were used to synthesize ZnO doped with 5, 10, 15 and 20 at.% Al or Ga. The resultant films showed

74   transparency greater than 80% and resistivities in the order of 10^{-3} Ωcm.[18] Earlier this year both Al

75   (1.5 at.%) and Ga (1.5 at.%) doped ZnO powders and thin films (produced *via* AACVD) were also reported with

76   resistivity values of 5.6×10^{-4} Ωcm and 5.7×10^{-3} Ωcm, respectively using a microwave assisted synthesis.[19]

77   In both of these reports, where commercially available precursors were used, carbon and/or chlorine

78   contamination was reported in the resultant materials.

79   Research into metal oxide thin film synthesis has been carried out hand in hand with the development of

80   metal-organic precursors, usually metal alkoxides or β-diketonates designed to limit contamination.[20]

81   These are single-source precursors containing a direct metal-oxygen bond that can either be synthesised or in

82   some cases are commercially available. β-ketoimine ligands can form a complex with a metal centre, forming

83   a delocalised ring including O and N donor atoms. The use of the ligand has been reported to increase

84   thermal stability and lower the melting point. The move from β-diketonates to β-dikeiminate facilitates the

85   incorporation of a N atom into the delocalised ring which can be further functionalised – allowing various

86   properties of the precursors to be tuned with the careful selection of R group on the N.[21] It has been shown

87   recently that varying the R group on the nitrogen atom in a range of β-diketoiminate ligands dramatically

88   altered the properties of the resultant aluminium and gallium containing precursors.[22]

89   The ability to isolate a precursor as an oil, can be advantageous, particularly for use in AACVD, where

90   precursors must be soluble in order to generate the aerosol mist.[9] Ligand modification is not limited to

91   functionalisation on the nitrogen atom, it can include the fluorination of the alkyl backbone; these electron

92   withdrawing groups can reduce the strength of the intermolecular forces *via* increased electron density at the

93   metal centre resulting in a more volatile product. However contamination and the risk of metal corrosion

94   from fluoride species must be taken into consideration.[3,20] A range of zinc β-diketoiminate compounds

95   have been successfully utilized in the CVD of ZnO films,[23,24] and it is proposed that an extension to this

96   groundwork could include the incorporation of Al and Ga dopants to improve the conductivity of the

97   resultant materials.

98   Previous reports of AZO and GZO synthesis describe chlorine contamination as a result of precursor ligand

99   design, in this paper, to circumnavigate this we combine the use of an identical β-diketoiminate ligand motif

100   on zinc, aluminium and gallium compounds with AACVD in order to facilitate doping into the ZnO lattice. The

101   use of the solution based technique, AACVD, overcomes the need for volatile precursors whilst the metal β-

102   diketoiminate precursors presented herein exhibit similar decomposition mechanisms. The precursors

103   therefore decompose cleanly, readily dope the ZnO framework (at 400 °C) and produce increasingly

104   conductive thin films of ZnO, GZO and AZO, respectively, free from chlorine contamination.

105   **2. Material and methods**

106   *2.1. Precursor synthesis*

107 ZnEt$_2$, AlEt$_3$ and GaMe$_3$ are pyrophoric substances that can ignite spontaneously in air and react violently with

108 water. Therefore, all reactions involving air sensitive materials were carried out under a dry dinitrogen

109 (99.99% from BOC) atmosphere using an MBraun glove box and Schlenk techniques. All experimental should

110 be conducted in a fume hood. Following the deposition films were air and moisture stable and were safe to

111 handle as any reactive species leave *via* the reactor exhaust during the AACVD process. All solvents used were

112 stored in alumina columns and dried, such that the water concentration was 5 – 10 ppm. AlEt$_3$ and GaMe$_3$

113 were procured from SAFC Hitech, ZnEt$_2$ and all other chemicals were purchased from Aldrich and stored

114 appropriately.

115 ^{1}H and ^{13}C NMR spectra were obtained on a Bruker AMX500 spectrometer, operating at 500.13 MHz, using

116 CD$_2$Cl$_2$ or CDCl$_3$ which were dried and degassed over molecular sieves prior to use; ^{1}H and ^{13}C chemical shifts

117 are reported relative to SiMe$_4$ (δ 0.00). IR spectra were recorded using a Shimadzu FTIR-8200 spectrometer,

118 operating in the region of 4000-400 cm^{-1}. Mass spectra were obtained using a Micromass 70-SE spectrometer

119 using Chemical Ionoisation (CI) with methane reagent gas. Elemental Analysis was carried using Elemental

120 Analyser (CE-440) (Exeter Analytical Inc). The instrument used for thermal analysis was a Netzsch Jupiter. All

121 measurements were carried out with the precursor sample sealed in an aluminium pan. The data was

122 recorded from room temperature to 600°C (see **S.I.**).

123 *Synthesis of the protonated ligand: [OC(Me)CHC(Me)NH(^{i}Pr))], [Zn(OC(Me)CHC(Me)N(^{i}Pr))$_2$] (1) and*

124 *[Et$_2$Al(OC(Me)CHC(Me)N(^{i}Pr))] (2) are consistent with literature and are included in* **S.3**.

125 *2.2. Synthesis of [Me$_2$Ga(OC(Me)CHC(Me)N(^{i}Pr))] (3)*

126 The β-ketoiminate ligand, [OC(Me)CHC(Me)NH(^{i}Pr))] (1.00 g, 7.0 mmol) in toluene (20 mL) was added

127 dropwise to a solution of GaMe$_3$ (0.81 g, 7.0 mmol) in toluene (20 mL) at −78°C. This was stirred overnight

128 and the solvent was removed *in vacuo* to yield a viscous yellow oily product **1** (70%). ^{1}H NMR δ/ppm (C$_6$D$_6$):

129 4.56 (s, 1H, COC*H*), 3.21 (m, 1H, C*H*(Me)$_2$), 1.66 (s, 3H, MeCO), 1.34 (s, 3H, CNMe), 1.10 (6H, d, NCH(Me)$_2$),

130 0.14 (4H, m, GaMe). ^{13}C{^{1}H} NMR δ/ppm 180.0 (CO), 165.2 (CN), 82.3 (CH), 39.7 (NC(Me)$_2$), 26.2 (OCMe), 23.5

131 (NC(Me)$_2$), 22.2 (COMe), 1.8 (GaMe). M/S: *m/z* [ES] + 239.99. Elemental anal. calc. %: C: 50.05, H: 8.40, N:

132 5.84, found %: C: 51.3, H: 9.1, N: 5.99.

133 *2.3. Chemical vapour deposition*

134 AACVD reactions took place within a fume hood. Depositions were carried out on SiO$_2$ coated barrier glass

135 substrates with proportions: 90 mm × 45 mm × 4 mm within a cold walled, horizontal bed reactor. Two glass

136 substrates were used to form a bottom plate which sat directly on top of the graphite heating block and a top

137 plate positioned above it with a 0.5 cm gap between them. The desired thin film was deposited on the

138 bottom plate, whilst the top plate reduces turbulence, ensuring laminar gas flow. The glass substrates were

139 cleaned thoroughly using water, ^{i}PrOH and acetone and then dried in air before each use. The temperature of

140 the graphite heating block was controlled using a platinum-rhodium thermocouple and the reactor was kept

141   under a flow of the N_2 carrier gas and the aerosol entering through the brass baffle. The reactor was sealed

142   with a cylindrical quartz tube capped by two stainless steel end plates with an exhaust. Before the aerosol

143   was formed, the precursor was weighed out into a glass bubbler and appropriate solvent added. Once the

144   reactor had reached the required temperature, the glass bubbler was attached to the reactor using PTFE

145   tubing *via* a one way glass T-piece. The flow meter, controlling the N_2 carrier gas flow, was diverted through

146   the T-piece diverting the aerosol mist generated by a humidifier into the reactor *via* the baffle. To create the

147   aerosol, an ultrasonic humidifier containing a piezoelectric device, which functions at 20 kHz was used. XRD

148   was carried out with a Bruker D8 Discover X-ray diffractometer using monochromatic Cu $K_{\alpha 1}$ and Cu $K_{\alpha 2}$

149   radiation of wavelengths 1.54056 and 1.54439 Å respectively, emitted in an intensity ratio of 2:1, voltage = 40

150   kV; current = 40 mA. SEM was performed using a Philips XL30 FEG with an electron beam accelerating energy

151   of 30 kV. XPS profiling was performed using a Thermo Scientific K-Alpha XPS system using monochromatic Al

152   K_{α} radiation at 1486.6 eV X-ray source. CasaXPS software was used to analyse the data with binding energies

153   referenced to an adventitious C 1s peak at 284.8 eV. UV/Vis/NIR transmission spectra were recorded using a

154   PerkinElmer Lambda 950 spectrometer in the range of 300 – 1400 nm with an air background.

155   *2.4. General procedures*

156   Due to the air sensitive nature of the precursors, standard Schlenk and glovebox (MBraun Unilab) techniques

157   were employed and all precursors and solvents were kept under a dry N_2 atmosphere. Solvents were added

158   to the vessel containing the precursor using an oven-dried cannula and then attached to the AACVD

159   apparatus under a flow of N_2. A number of different flow rates were tested ranging between 1-2 L/min as

160   well as a variety of different deposition temperatures. The AACVD reaction lasted between 30-60 min and the

161   reactor was set to cool to room temperature, still under a flow of N_2. Many attempts were made to optimise

162   the AACVD reaction of the precursor testing different solvents, flow rates, temperatures and masses of

163   precursor.

164   *2.5. AACVD of ZnO from **1***

165   **1** (0.2 g, 0.578 mmol) was added to a glass flask in the glove box. A small amount of CH_2Cl_2 (ca. 10 mL) was

166   added to dissolve the precursor followed by toluene (*ca.* 30 mL). The resultant solution was a transparent,

167   pale yellow/orange colour. The AACVD reactor was heated to 400 °C whilst under a flow of N_2 gas at a flow

168   rate of 1 L/min. The flow of N_2 was then diverted into the glass bubbler through the precursor solution

169   allowing the aerosol mist to be directed into the AACVD reactor. The deposition took 30 min and the reactor

170   was cooled to room temperature under a flow of N_2 gas before the substrate was removed.

171   *2.6. AACVD of AZO, GZO and $GaZn_2O_4$.*

172   The experimental procedure described above was repeated several times, films of AZO from one-pot of **1** and

173   **2** in a 1:0.05 ratio (0.5 mmol scale). GZO films were deposited as above using compounds **1** and **3** (also one-

174   pot) in a ratio of 1:0.05 (0.5 mmol scale). The experimental procedure described for GZO was repeated with

175   the addition of a piece of glass quartz (2 cm × 2 cm) placed on top of the substrate. The quartz was then

176   transferred to a Carbolite cwf 13/13 furnace and annealed at 1000 °C overnight, in order to carry out XRD

177   analysis.

178   **3. Results and discussion**

179   *3.1. Synthesis of **1**-**3***

180   β-ketoimine compounds, formed in a simple condensation reaction have been widely explored as ligands for

181   a range of metals and used in the synthesis of successful precursors for metal oxide thin films.[22,23]

182   Following the synthesis and isolation of the ligand, [(Me)CN(H){^{i}Pr}–CHC(Me)=O], two equivalents were

183   reacted with diethyl zinc in toluene and a white precipitate of **1** was obtained and isolated in good yield, after

184   being filtered and washed with hexane. Conversely compounds **2** and **3** were not isolated as precipitates after

185   an overnight reflux of a 1:1 reaction of the aforementioned ligand with AlEt$_3$ and GaMe$_3$ which yielded oils of

186   **2** and **3**, respectively. Formation of **1** and **2** were confirmed *via* ^{1}H, ^{13}C, MS and EA and were consistent with

187   literature.[22,23] The proton resonances in the NMR of **3** for the Ga-ligand environments were significantly

188   shifted from ^{1}H environments observed for the protonated ligand: [(Me)CN(H){^{i}Pr}–CHC(Me)=O] alone,

189   evidencing the formation of **3**. Elemental analysis and mass spectrometry confirm the isolation of **3**,

190   futhermore, the 2:1 ratio of methyl group proton environments to the Ga-ligand proton environments in the

191 ^{1}H NMR support the formation of **3** (Scheme 1).
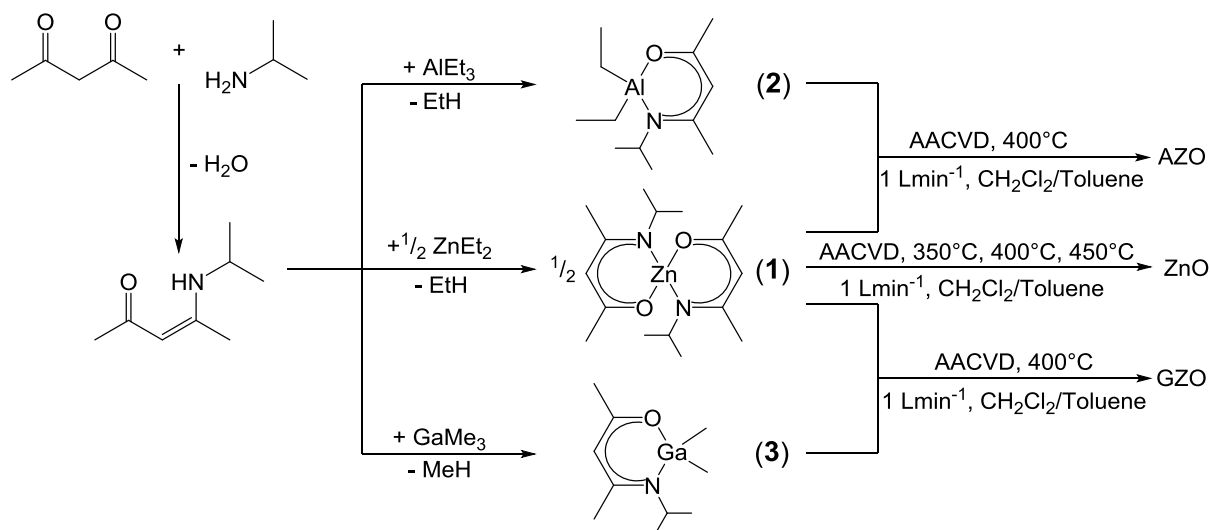
192
193   **Scheme 1**. Synthesis of β-ketoiminate metal complexes **1**-**3** and the conditions for the AACVD of thin films of

194   ZnO, AZO and GZO.

195   *3.2. AACVD of ZnO, AZO and GZO*

196   Following optimisation of the AACVD process (see **S.I.**) compound **1** was used to deposit thin films of ZnO at

197   400 °C. Films of AZO were achieved at 400 °C *via* a one-pot AACVD charged with **1** and **2** in a 1:0.05 ratio.

198   Following the procedure for the synthesis of thin films of AZO (at 400 °C), GZO films were also successfully

199 deposited using compounds **1** and **3** in a ratio of 1:0.05. For all films the CH_2Cl_2/toluene solvent system was
200 utilised (see **S.I.**). The films of ZnO, AZO and GZO were transparent displaying a slight brown tinge, indicative
201 of carbon contamination. All films were adherent to the glass substrate after wiping, scratching with a scalpel,
202 the scotch tape test and treating with acetone and other organic solvents. The films perished when left in
203 nitric acid overnight.

204
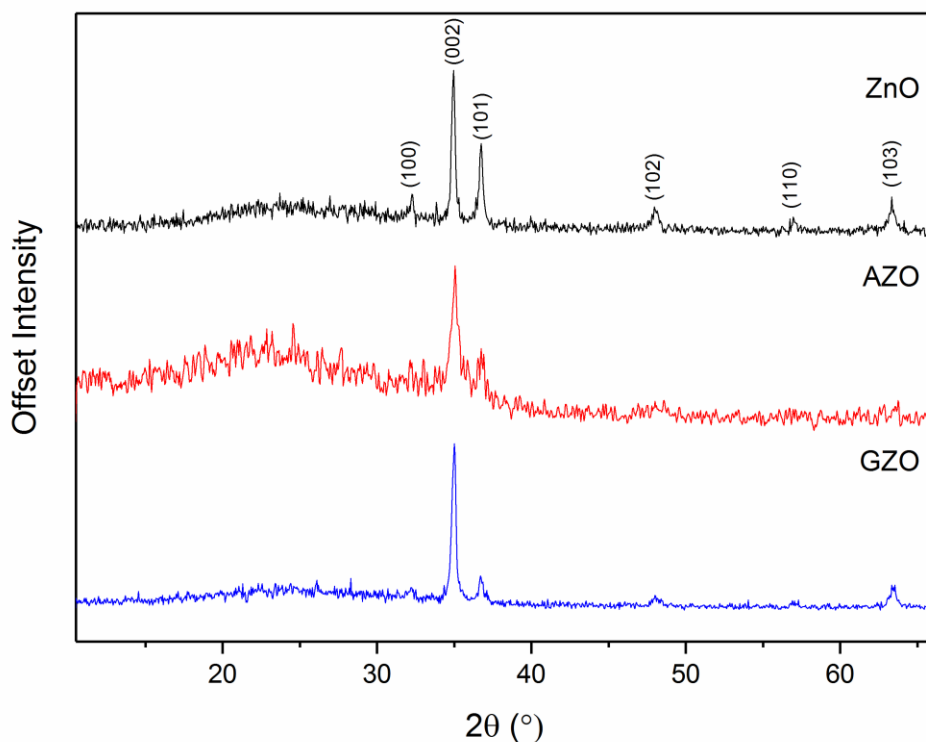
Fig. 1: XRD pattern showing: ZnO deposited by AACVD of **1** at 400°C (black);[10] AZO deposited from **1** and **2**
206 (red); GZO deposited from **1** and **3** (blue). Peaks verify the hexagonal wurzite structure expected.

207 The XRD pattern for films deposited from **1** show alignment to peaks typical of zinc oxide, with preferential
208 orientation for the (002) peak indicating orientation along the c axis.[25] Using the Le Bail method in GSAS,
209 the lattice parameters of the ZnO films were determined to be a = 3.2367(5) Å and b = 5.1613(5) Å.

210 AZO films deposited from a one-pot mixture of **1** and **2** show a significant decrease in peak intensity with Al
211 doping in their XRD pattern. This may be due to the varying film thickness which is well known to affect the
212 intensity of the XRD peaks. A shift in the peak position when doping occurs due to the change in lattice
213 parameters that accompanies the introduction of dopant atom into the host matrix, shifting was observed
214 when compared to the 2θ values of the undoped zinc oxide films. Firstly for the (002) peak from 34.85° to
215 35.00° 2θ and the (100) peak from 31.40° to 32.15° 2θ. The replacement of Zn^{2+} ions with the smaller Al^{3+} ions
216 caused a shift of the (100) peak to a larger 2θ.[26] Lattice parameters of the unit cell were calculated for AZO

217 films to investigate the effect of doping on the crystal structure. Using the aforementioned methods the

218 lattice parameters were determined to be a = 3.2353(5) Å and b = 5.1785(5) Å.

219 In the XRD patterns of films of GZO deposited from one-pot mixtures of **1** and **3** preferential orientation

220 remained for the (002) peak, and the intensity of the peaks was decreased in comparison with undoped ZnO.

221 A very slight shift in the (002) peak was observed in the spectrum from 34.85° in the undoped ZnO film to

222 34.9° 2θ in the GZO. However, the difference in size between the ionic radii of zinc and gallium is relatively

223 small, therefore shifting may not occur as the distortion of the crystal lattice could be minimal, with similar

224 observations have been reported in the literature.[14] The shift is smaller than that observed for the AZO

225 films which is expected due to the smaller difference in ionic radii between zinc and gallium compared to that

226 of zinc and aluminium.

227 As with AZO, lattice parameters of the unit cell were calculated for GZO films to investigate the effect of

228 doping on the crystal structure. Using the Le Bail method lattice parameters were determined to be

229 a = 3.2257(5) Å and b = 5.1496(5) Å. The data reveals a slight shift in the parameters showing a small effect on

230 the crystal structure by the dopant atoms. In the case of gallium, it is well reported in the literature that

231 incorporation into the ZnO crystal structure causes the (002) to shift to a higher angle side, reflected in the

232 decrease in the c parameter from 5.16 Å to 5.15 Å.[27]

233 Energy dispersive X-ray (EDX) analysis of films of ZnO deposited from **1** confirmed the presence of zinc but

234 could not be used to give a metal to oxygen ratio due to breakthrough to the substrate. Carbon

235 contamination was apparent from the EDX data (~ 15 at.% carbon). The EDX analysis of the AZO films

236 confirmed the Al content of the films to be 4.8 at.%, closely corroborating the experimental concentrations

237 used. Films of GZO deposited from **1** and **3** were analysed by EDX and shown to contain 4.5 at.% Ga, in both

238 the AZO and GZO films carbon content was below 5 at.% (approaching detection limit) no chlorine

239 contamination could be detected.
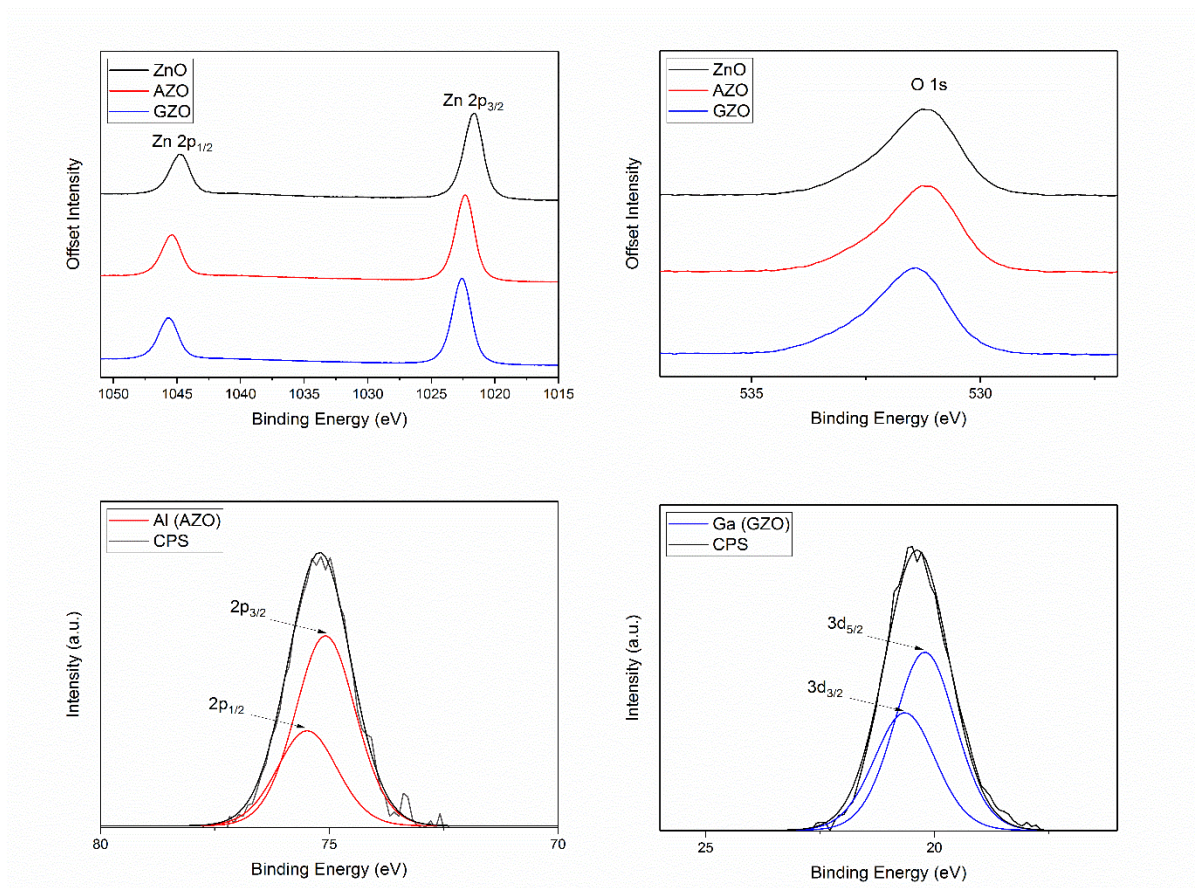
Fig. 2: XPS analysis of: Zn 2p peaks in ZnO (black), AZO (red) and GZO (blue) (top left); O 1s peaks in ZnO (black), AZO (red) and GZO (blue) (top right); Al 2p in AZO (red) (bottom left); and Ga 3d in GZO (blue) (bottom right).

In the X-ray photoelectron spectroscopy (XPS) data all peaks were fitted by a Gaussian/Lorentzian product distribution. For films deposited from **1** a Zn:O ratio of 1.1:1.0 was calculated, indicative of binary ZnO with a Zn $2p_{3/2}$ binding energy of 1021.5 eV.[28] In Fig. 2 (top left) the Zn 2p peaks are offset for ZnO (black), AZO (red) and GZO (blue), a slight shift, consistent with the presence of Al and Ga dopants, respectively, was observed for the Zn $2p_{3/2}$ binding energy: 1022.7 eV (AZO) and 1022.3 eV (GZO). The O 1s spectra recorded for the ZnO, AZO and GZO films (Fig. 2, top right) all included a peak located between 530-534 eV. This can be assigned to O^{2-} ions in the ZnO hexagonal wurtzite structure. The appearance of a shoulder in each of the spectra correspond to the presence of loosely bound surface species.

XPS confirmed the presence of Al(III) in the AZO films deposited from **1** and **2**, the binding energy of Al $2p_{3/2}$ was 75.1 eV and the Al $2p_{1/2}$ was 75.5 eV (Fig. 2, bottom left), higher than previous reports for Al_2O_3,[22] which is consistent for Al as a dopant as opposed to when incorporated within its binary oxide.[29] In the XPS of the GZO films deposited from **1** and **3**, the binding energy of the Ga $3d_{5/2}$ at 20.2 eV is indicative of Ga(III) (Fig. 2, bottom right). Since this technique only probes the surface and not the bulk of the material and this,

257 combined with the issues associated with the low doublet splitting in the Al 2p and Ga 3d ionizations, at% of
258 aluminium or gallium could not be calculated from the XPS data.[30]
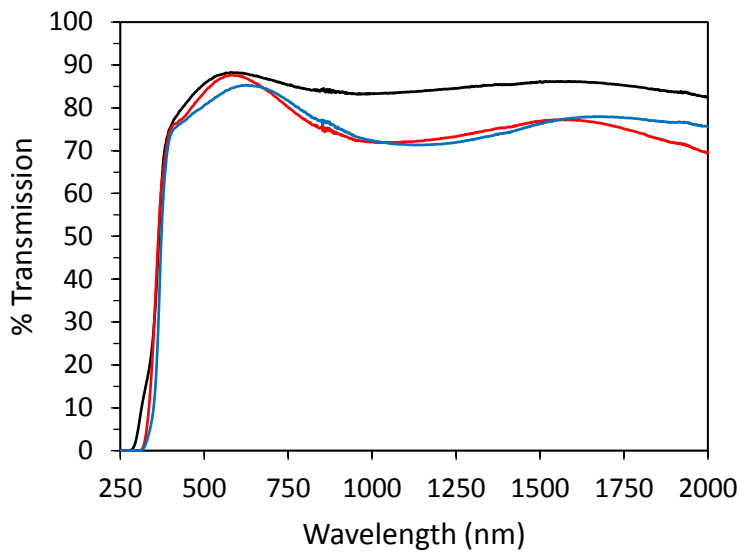
259 **Fig. 3**: UV/vis data for ZnO thin film deposited from **1** at 400°C (black); AZO film deposited from **1** and **2** at
260 400°C (red); GZO film deposited from **1** and **3** at 400°C (blue).

261 Using UV/Vis spectroscopy, it was possible to obtain information using transmission reflectance data about
262 the transparency and bandgap of the thin films of ZnO, AZO and GZO by using a Tauc plot. A value of 3.13 eV
263 was calculated in accordance with literature values for the band gap of the thin films of ZnO deposited using
264 **1**.[9] Comparatively the band gap of the AZO films deposited from compounds **1** and **2** and the GZO films
265 deposited from **1** and **3** were found to be 3.25 and 3.28 eV respectively. The increase in the bandgap upon
266 doping may be expected due to an increased charge carrier concentration due to the Burnstein-Moss effect
267 widening the bandgap.[14] The slightly wider band gap contributes to the high optical transparency of the
268 films. The data showed transmission exceeded 80% in all films in the visible region fitting the requirements
269 for a TCO.

270 Resistance of the films was determined by two-point probe, additionally, using the film thickness obtained
271 from Filmetrics equipment the resistivity was calculated. Table 1 summarises the data for the ZnO, AZO and
272 GZO films.[26]

273 **Table 1**
274 Summary of the characterisation of ZnO, AZO and GZO thin films: film thickness (d), sheet resistance (R_{Sh}),
275 bulk resistivity (ρ), cell parameters were calculated using a Le Bail refinement, position of the (002) peak in
276 the XRD pattern (°), band gap (E_g), at.% of dopant from EDX.

Film	d (nm)	R_{Sh} ($k\Omega sq^{-1}$)	ρ (Ωcm)	Cell parameters (Å)	(002) Peak position (°)	E_g (eV)	EDX (at%)

ZnO	182.6	70	1.270	a = 3.2367(5) b = 5.1613(5)	34.85	3.13	-
AZO	210.3	12	0.252	a = 3.2353(5) b = 5.1785(5)	35.00	3.25	4.8 (Al)
GZO	189.1	40	0.756	a = 3.2257(5) b = 5.1496(5)	34.90	3.28	4.5 (Ga)

277 A lower resistivity was recorded in the doped films compared to the ZnO indicating that the addition of

278 dopant improved the electrical properties significantly (Table 1). However, the effect of film thickness must

279 be noted and although not a direct correlation, thicker films generally had better conductivity.
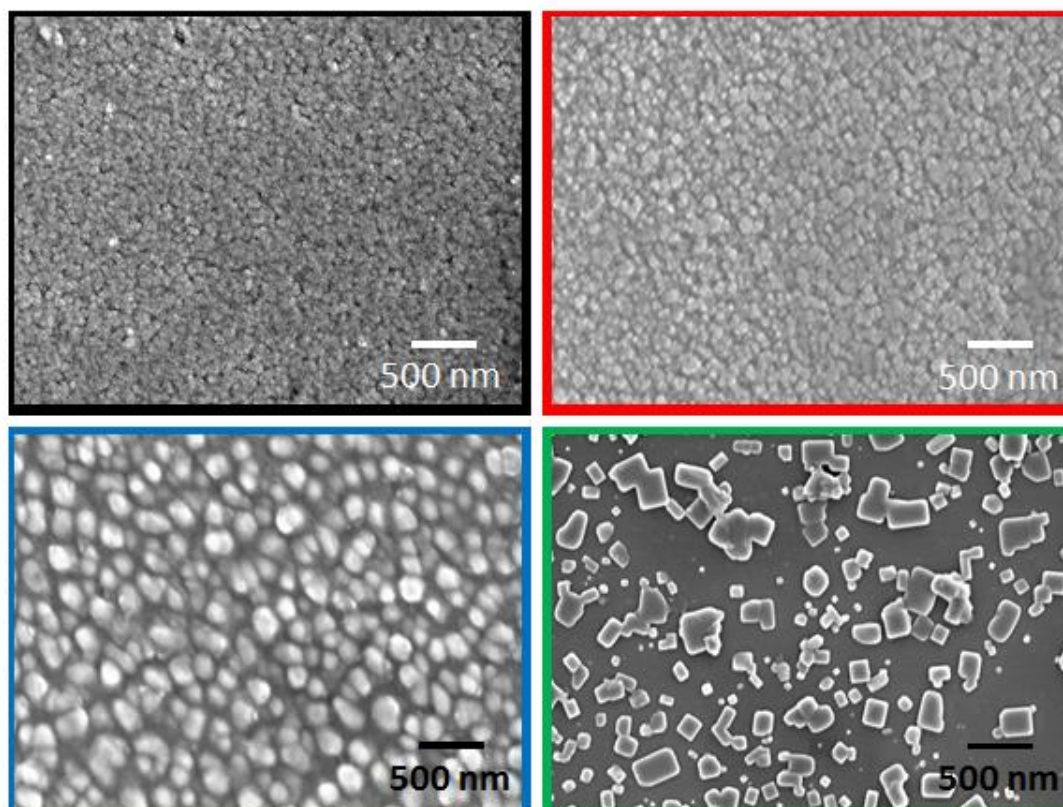
280

281 **Fig. 4**: SEM images of thin films grown at 400°C of: ZnO deposited from **1** (black border); b) AZO deposited

282 from a one-pot mixture of **1** and **2** (red border); GZO deposited from a one-pot mixture of **1** and **3** (blue

283 border); and the crystalline spinel: GaZn$_2$O$_4$ produced from heating GZO thin films on quartz substrates at

284 1000°C (green border).

285 Scanning electron microscopy (SEM) shows the surface morphology of the zinc oxide films deposited from **1**

286 (Fig. 4, black border) to be similar in appearance from the AZO films indicating that doping, in this instance

287 seems to have little effect on the morphology. Interestingly however the GZO films appeared to be formed of

288 larger spherical units (Fig. 4, blue border). These GZO films were also deposited on quartz and then annealed

289 at 1000 °C. The relatively equally sized clusters (~70 nm) observed on the GZO films were replaced with an

290 array of crystalline blocks, after annealing (Fig. 4, green border).

291 *3.3. Investigation of the Kirkendall Effect*

292 The Kirkendall effect - namely bulk diffusion at the interface of two metal layers which produces both

293 vacancies and new materials - has been exploited in recent years for the synthesis of hollow

294 nanomaterials.[31,32] A mechanism analogous to this effect has been used to synthesize spinel structures of

295 the type AB_2O_4, from a range of techniques including ALD and CVD whereby layers of different materials are

296 heated above a certain temperature.[33–35] It is likely that the GZO films presented herein have an

297 amorphous layer of oxide at their surface. This can be difficult to detect in films deposited at 400 °C because

298 Ga_2O_3 is amorphous at this temperature ruling out XRD analysis, furthermore the low doublet separation in

299 the XPS for gallium implies that any number of environments can fit the single peak recorded.

300 In order to investigate the effect this layer may have on the material beneath, films of GZO were annealed at

301 1000 °C. The XRD data below (Fig. 5) confirms the spinel zinc gallate, $ZnGa_2O_4$ formed alongside Ga_2O_3.

302 Annealing the film had therefore caused the formation of $ZnGa_2O_4$ from a reaction between Ga_2O_3 present on

303 the surface and the underlying GZO.[29]

304
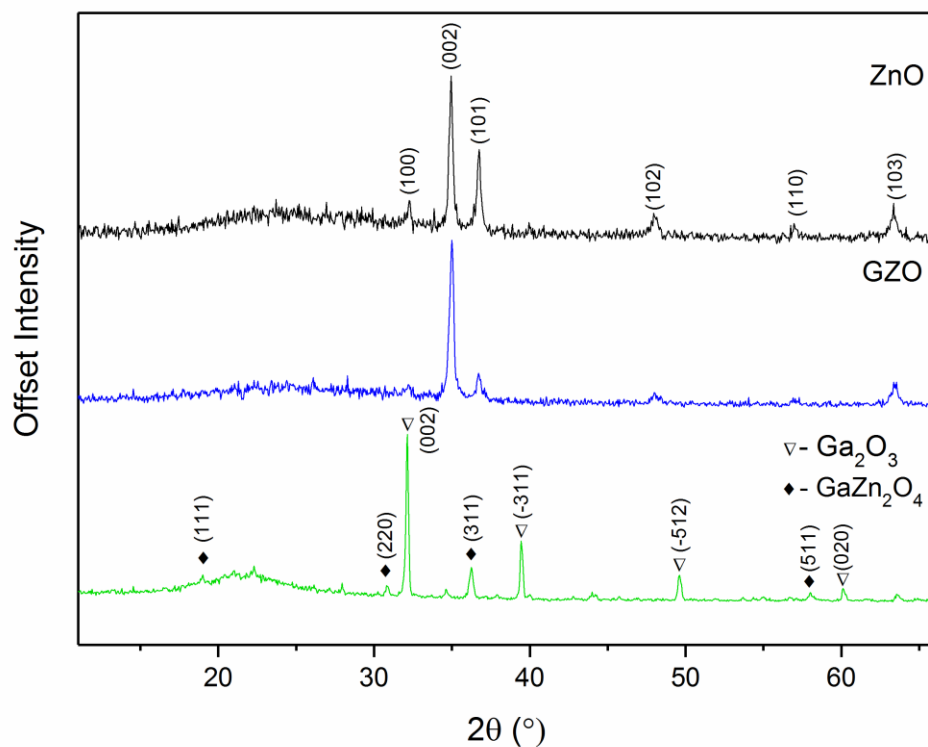
305

306 **Fig 5**: XRD spectra of ZnO on glass (black); GZO film deposited on glass (blue) and GZO on quartz annealed at

307 1000°C (green). Diamond markers in the annealed spectrum show where Bragg peaks occur characteristic of

308 zinc gallate, triangle markers show Ga_2O_3.

309 Ga_2O_3 and $GaZn_2O_4$ are the thermodynamically stable products at 1000 °C when compared to GZO. These

310 results confirm AACVD as a simple alternative to some multistep processes[5] which are currently used to

311 deposit spinels consistent with previous investigations into post-annealing temperatures.[36]

312 **4. Conclusions**

313 Following the synthesis of zinc, aluminium and gallium containing compounds using the same β-ketoimine

314 ligand – each containing pre-formed metal-oxygen bonds, AACVD has been used to deposit in a simple one

315 step procedure thin films of ZnO, AZO and GZO. Films were deposited on glass at 400 °C, and in the case of

316 GZO, also on quartz for post-annealing treatment confirming the formation of the thermodynamically

317 favourable spinel $GaZn_2O_4$. Dopant concentration in the films matches the amount added to the reaction pot,

318 proving this to be an efficient and non-wasteful technique. In conclusion the thin films deposited using these

319 precursors showed reasonable electrical conductivity and showed excellent optical properties; a promising

320 proof of concept for one-pot made-to-measure precursor systems.

323 **6. References**

324 [1] C.E. Knapp, C.J. Carmalt, Solution based CVD of main group materials, Chem Soc Rev. 45 (2016)
325   1036–1064. doi:10.1039/C5CS00651A.
326 [2] B.G. Lewis, D.C. Paine, Applications and Processing of Transparent Conducting Oxides, MRS
327   Bull. 25 (2000) 22–27. doi:10.1557/mrs2000.147.
328 [3] Y.-H. Liu, Y.-C. Cheng, Y.-L. Tung, Y. Chi, Y.-L. Chen, C.-S. Liu, S.-M. Peng, G.-H. Lee,
329   Synthesis and characterization of fluorinated ??-ketoiminate and imino-alcoholate Pd
330   complexes: precursors for palladium chemical vapor deposition, J. Mater. Chem. 13 (2003)
331   135–142. doi:10.1039/b208535f.
332 [4] S.-U. Park, J.-H. Koh, Electrical and optical properties of in and Al doped ZnO thin film, Electron.
333   Mater. Lett. 9 (2013) 493–496. doi:10.1007/s13391-013-0046-9.
334 [5] E. Fortunato, L. Raniero, L. Silva, A. Goncalves, A. Pimentel, P. Barquinha, H. Aguas, L. Pereira,
335   G. Goncalves, I. Ferreira, Highly stable transparent and conducting gallium-doped zinc oxide
336   thin films for photovoltaic applications, Sol. Energy Mater. Sol. Cells. 92 (2008) 1605–1610.
337   doi:10.1016/j.solmat.2008.07.009.
338 [6] S.Y. Li, P. Lin, C.Y. Lee, T.Y. Tseng, C.J. Huang, Effect of Sn dopant on the properties of ZnO
339   nanowires, J. Phys. Appl. Phys. 37 (2004) 2274–2282. doi:10.1088/0022-3727/37/16/009.
340 [7] A. Hafdallah, F. Yanineb, M.S. Aida, N. Attaf, In doped ZnO thin films, J. Alloys Compd. 509
341   (2011) 7267–7270. doi:10.1016/j.jallcom.2011.04.058.
342 [8] V.R. Shinde, T.P. Gujar, C.D. Lokhande, R.S. Mane, S.-H. Han, Mn doped and undoped ZnO
343   films: A comparative structural, optical and electrical properties study, Mater. Chem. Phys. 96
344   (2006) 326–330. doi:10.1016/j.matchemphys.2005.07.045.
345 [9] K. Ellmer, Resistivity of polycrystalline zinc oxide films: current status and physical limit, J. Phys.
346   Appl. Phys. 34 (2001) 3097–3108. doi:10.1088/0022-3727/34/21/301.
347 [10] M.N. Islam, T.B. Ghosh, K.L. Chopra, H.N. Acharya, XPS and X-ray diffraction studies of
348   aluminum-doped zinc oxide transparent conducting films, Thin Solid Films. 280 (1996) 20–25.
349   doi:10.1016/0040-6090(95)08239-5.
350 [11] D.P. Howard, P. Marchand, L. McCafferty, C.J. Carmalt, I.P. Parkin, J.A. Darr, High-
351   Throughput Continuous Hydrothermal Synthesis of Transparent Conducting Aluminum and
352   Gallium Co-doped Zinc Oxides, ACS Comb. Sci. 19 (2017) 239–245.
353   doi:10.1021/acscombsci.6b00118.
354 [12] C.M. Muiva, T.S. Sathiaraj, K. Maabong, Effect of doping concentration on the properties of
355   aluminium doped zinc oxide thin films prepared by spray pyrolysis for transparent electrode
356   applications, Ceram. Int. 37 (2011) 555–560. doi:10.1016/j.ceramint.2010.09.042.

357   [13] L. Schmidt-Mende, J.L. MacManus-Driscoll, ZnO – nanostructures, defects, and devices, Mater.
358   Today. 10 (2007) 40–48. doi:10.1016/S1369-7021(07)70078-0.
359   [14] M.-C. Jun, S.-U. Park, J.-H. Koh, Comparative studies of Al-doped ZnO and Ga-doped ZnO
360   transparent conducting oxide thin films, Nanoscale Res. Lett. 7 (2012) 639. doi:10.1186/1556-
361   276X-7-639.
362   [15] E. Fortunato, D. Ginley, H. Hosono, D.C. Paine, Transparent Conducting Oxides for
363   Photovoltaics, MRS Bull. 32 (2007) 242–247. doi:10.1557/mrs2007.29.
364   [16] S. Chen, G. Carraro, D. Barreca, R. Binions, Growth and electro-optical properties of Ga-doped
365   ZnO films prepared by aerosol assisted chemical vapour deposition, Thin Solid Films. 584
366   (2015) 316–319. doi:10.1016/j.tsf.2014.11.092.
367   [17] S.D. Ponja, S. Sathasivam, I.P. Parkin, C.J. Carmalt, Transparent conductive aluminium and
368   fluorine co-doped zinc oxide films via aerosol assisted chemical vapour deposition, RSC Adv. 4
369   (2014) 49723–49728. doi:10.1039/C4RA09997D.
370   [18] D.B. Potter, D.S. Bhachu, M.J. Powell, J.A. Darr, I.P. Parkin, C.J. Carmalt, Al-, Ga-, and In-
371   doped ZnO thin films via aerosol assisted CVD for use as transparent conducting oxides: Al-,
372   Ga-, and In-doped ZnO thin films via aerosol assisted CVD, Phys. Status Solidi A. 213 (2016)
373   1346–1352. doi:10.1002/pssa.201532996.
374   [19] D.S.Y. Jayathilake, T.A.N. Peiris, J.S. Sagu, D.B. Potter, K.G.U. Wijayantha, C.J. Carmalt, D.J.
375   Southee, Microwave-Assisted Synthesis and Processing of Al-Doped, Ga-Doped, and Al, Ga
376   Codoped ZnO for the Pursuit of Optimal Conductivity for Transparent Conducting Film
377   Fabrication, ACS Sustain. Chem. Eng. 5 (2017) 4820–4829.
378   doi:10.1021/acssuschemeng.7b00263.
379   [20] D. Pugh, P. Marchand, I.P. Parkin, C.J. Carmalt, Group 13 β-Ketoiminate Compounds: Gallium
380   Hydride Derivatives As Molecular Precursors to Thin Films of Ga_2O_3, Inorg. Chem. 51 (2012)
381   6385–6395. doi:10.1021/ic3006794.
382   [21] P. Marchand, C.J. Carmalt, Molecular precursor approach to metal oxide and pnictide thin films,
383   Coord. Chem. Rev. 257 (2013) 3202–3221. doi:10.1016/j.ccr.2013.01.030.
384   [22] C.E. Knapp, P. Marchand, C. Dyer, I.P. Parkin, C.J. Carmalt, Synthesis and characterisation of
385   novel aluminium and gallium precursors for chemical vapour deposition, New J Chem. 39
386   (2015) 6585–6592. doi:10.1039/C5NJ00947B.
387   [23] J.S. Matthews, O.O. Onakoya, T.S. Ouattara, R.J. Butcher, Synthesis and characterization of
388   zinc AP-MOCVD precursors and their utility in the growth of ZnO, Dalton Trans. (2006) 3806.
389   doi:10.1039/b603308c.
390   [24] J. Holmes, K. Johnson, B. Zhang, H.E. Katz, J.S. Matthews, Metal organic chemical vapor
391   deposition of ZnO from β-ketoiminates: MOCVD of ZnO from β-ketoiminates, Appl.
392   Organomet. Chem. 26 (2012) 267–272. doi:10.1002/aoc.2850.
393   [25] Z.R. Khan, Optical and Structural Properties of ZnO Thin Films Fabricated by Sol-Gel Method,
394   Mater. Sci. Appl. 02 (2011) 340–345. doi:10.4236/msa.2011.25044.
395   [26] S.S. Meysami, A.A. Koós, F. Dillon, N. Grobert, Aerosol-assisted chemical vapour deposition
396   synthesis of multi-wall carbon nanotubes: II. An analytical study, Carbon. 58 (2013) 159–169.
397   doi:10.1016/j.carbon.2013.02.041.
398   [27] S. Liang, Z.-X. Mei, X.-L. Du, Modulation of electrical and optical properties of gallium-doped
399   ZnO films by radio frequency magnetron sputtering, Chin. Phys. B. 21 (2012) 067306.
400   doi:10.1088/1674-1056/21/6/067306.
401   [28] H.A. Ali, A.A. Iliadis, A. Von Cresce, P. Kofinas, U. Lee, Properties of self-assembled ZnO
402   nanostructures on Si and SiO/sub 2/ wafers, in: IEEE, 2001: pp. 454–457.
403   doi:10.1109/ISDRS.2001.984543.
404   [29] J.-L. Yan, Y.-N. Zhao, C. Li, Formation of $ZnGa_2O_4$ films by multilayer deposition and
405   subsequent thermal annealing, Chin. Phys. B. 23 (2014) 048105. doi:10.1088/1674-
406   1056/23/4/048105.
407   [30] J. Creighton, Ho, P, Introduction to chemical vapor deposition (CVD), ASM International,
408   Materials Park, OH, 2001.
409   [31] H.J. Fan, M. Knez, R. Scholz, D. Hesse, K. Nielsch, M. Zacharias, U. Gösele, Influence of
410   Surface Diffusion on the Formation of Hollow Nanostructures Induced by the Kirkendall Effect:
411   The Basic Concept, Nano Lett. 7 (2007) 993–997. doi:10.1021/nl070026p.

412 [32] H. Jin fan, M. Knez, R. Scholz, K. Nielsch, E. Pippel, D. Hesse, M. Zacharias, U. Gösele,
413   Monocrystalline spinel nanotube fabrication based on the Kirkendall effect, Nat. Mater. 5
414   (2006) 627–631. doi:10.1038/nmat1673.
415 [33] C.E. Knapp, J.A. Manzi, A. Kafizas, I.P. Parkin, C.J. Carmalt, Aerosol-Assisted Chemical
416   Vapour Deposition of Transparent Zinc Gallate Films, ChemPlusChem. 79 (2014) 1024–1029.
417   doi:10.1002/cplu.201402037.
418 [34] C.E. Knapp, I.D. Prassides, S. Sathasivam, I.P. Parkin, C.J. Carmalt, Aerosol-Assisted Chemical
419   Vapour Deposition of a Copper Gallium Oxide Spinel, ChemPlusChem. 79 (2014) 122–127.
420   doi:10.1002/cplu.201300289.
421 [35] S. Kumar, G. Sarau, C. Tessarek, M. Göbelt, S. Christiansen, R. Singh, Study of high quality
422   spinel zinc gallate nanowires grown using CVD and ALD techniques, Nanotechnology. 26
423   (2015) 335603. doi:10.1088/0957-4484/26/33/335603.
424 [36] C.H. Ahn, S.H. Kim, Y.K. Kim, H.S. Lee, H.K. Cho, Effect of post-annealing temperatures on
425   thin-film transistors with ZnO/Al2O3 superlattice channels, Thin Solid Films. 584 (2015) 336–
426   340. doi:10.1016/j.tsf.2015.01.017.
427
428